Critical role of electrical resistivity in magnetoionics

de Rojas, J.; Salguero, J.; Quintana, A.; Lopeandia, A.; Liedke, M. O.; Butterling, M.; Elsherif, A. G. A.; Hirschmann, E.; Wagner, A.; Abad, L.; Costa-Krämer, J. L.; Sort, J.; Menéndez, E.;

Originally published:

September 2021

Physical Review Applied 16(2021), 034042

DOI: https://doi.org/10.1103/PhysRevApplied.16.034042

The critical role of electrical resistivity in magneto-ionics

Julius de Rojas, Joaquín Salguero, Alberto Quintana, Aitor Lopeandia, Maciej O. Liedke, Maik Butterling, Ahmed G. Attallah, Eric Hirschman, Andreas Wagner, Llibertat Abad, José L. Costa-Krämer, Jordi Sort* and Enric Menéndez**

Dr. Julius de Rojas, Prof. Aitor Lopeandia, Prof. Jordi Sort, Dr. Enric Menéndez
Departament de Física, Universitat Autònoma de Barcelona, E-08193 Cerdanyola del Vallès, Spain
E-mail: jordi.sort@uab.cat (Jordi Sort), enric.menendez@uab.cat (Enric Menéndez)

Joaquín Salguero, Prof. José L. Costa-Krämer
IMN-Instituto de Micro y Nanotecnología (CNM-CSIC), Isaac Newton 8, PTM, 28760 Tres Cantos, Madrid, Spain
E-mail: jl.costa.kramer@csic.es (José L. Costa-Krämer)

Dr. Alberto Quintana
Department of Physics, Georgetown University, Washington, D.C. 20057, United States

Prof. Aitor Lopeandia
Catalan Institute of Nanoscience and Nanotechnology (ICN2), Campus UAB, Bellaterra, Barcelona, 08193, Spain

Dr. Maciej O. Liedke, Dr. Maik Butterling, Dr. Ahmed G. Attallah, Dr. Eric Hirschman, Dr. Andreas Wagner
Institute of Radiation Physics, Helmholtz-Zentrum Dresden – Rossendorf, Dresden 01328, Germany

Dr. Llibertat Abad
Institut de Microelectrònica de Barcelona, IMB-CNM (CSIC), Campus UAB, E-08193 Bellaterra, Spain

Prof. Jordi Sort
Institució Catalana de Recerca i Estudis Avançats (ICREA), Pg. Lluís Companys 23, E-08010 Barcelona, Spain

Keywords: voltage control of magnetism, magneto-ionics, electric resistivity, electrolyte-gating, transition metal nitrides, nitrogen ions, open volume defects

The critical role of electrical resistivity in governing ion motion in magneto-ionic thin-film systems is demonstrated. A series of highly nanocrystalline cobalt-nitride (Co-N) thin films (85 nm thick) with similar composition but a broad range of electrical properties exhibit markedly different magneto-ionic behavior. Semiconducting, near stoichiometric films show the best performance, better than their metallic- and insulating- counterparts. Resistivity

reflects the interplay between atomic bonding, carrier localization and structural defects, which in turn determines the strength and distribution of applied electric fields inside the actuated films. This fact, generally overlooked, reveals that resistivity is a good indicator of the potential of a system to exhibit optimal magneto-ionic effects, while also opening interesting challenges.

1. Introduction

Modern magnetoelectronic devices, including micro-/nano-electromechanical systems (MEMS/NEMS), hard disk drives (HDDs), magnetoresistive random-access memories (MRAMs), etc., are ultimately modulated using electric currents, resulting in significant energy losses through heat dissipation. Voltage-controlled magnetism (VCM), utilizing voltage instead of current to manipulate magnetic properties, might lead to a significant reduction in energy consumption.[1,2] Thus, research in new micro-/nano-materials and magnetic actuation methods is critical for developing future miniaturized devices and technologies. Much research has been focused on magneto-ionics,[3–16] where ions (including O, Li, H, F or N) are moved into and out of a target material under an applied electric field, producing large, tunable, non-volatile changes in magnetic properties, including coercivity, exchange bias field, magnetic easy axis, or anisotropy.[6,7,10,14,17–23] Magneto-ionic structures are often constituted of ferromagnetic (FM) materials adjacent to an oxide layer which acts as a solid-state oxygen-ion reservoir, such as GdO_x or HfO_x. However, such FM/reservoir bilayer systems often suffer from poor cyclability due to irreversible structural changes undergone by the ferromagnetic metal in the oxidation/reduction process, which involves the formation/destruction of interfacial oxide phases.

An alternative is the use of single-layer target materials whose crystal structure already contains the ions to be transported (such as oxygen or nitrogen) in the as-prepared state (*e.g.*, Co_3O_4 or CoN).[8,10,24] Such target materials can undergo fully reversible transformations from

a non-ferromagnetic (OFF) to a ferromagnetic (ON) state and *vice versa* while experiencing less detrimental structural changes than the abovementioned magneto-ionic approaches, possibly due to Co_3O_4 or CoN structures providing "ready-made" lattice sites into which ions can be driven, leading to higher endurance. In contrast to Co_3O_4, where oxygen migration is assisted by the formation of filamentary channels,[10] room-temperature ON-OFF ferromagnetism in CoN films operates via front-like plane wave ionic motion, at lower applied voltages and with enhanced cyclability.[24] Thus, transition metal nitrides compare favorably with their transition metal oxide counterparts for magneto-ionic applications.

The magneto-ionic effects induced in either single-layer (Co_3O_4, CoN)[8] or bilayered (Co/GdO_x)[14] systems have been reported to depend on the occurrence of grain boundaries and vacancies (*i.e.*, grain boundaries act as paths for enhanced ionic diffusion[10]), which can be regarded as a tunable component. However, structural defects in general can induce scattering of electrons and therefore changes in electric resistivity,[25] which in turn affect the strength of the induced electric field inside the actuated material. The cohesive energy and the strength of interatomic bonds are also key parameters affecting magneto-ionic performance, as they are related to the energy required to dissociate cations and anions under the application of electric fields.[24] All these factors (structural defects, grain boundaries, type and strength of atomic bonding) determine electric conductivity.[26–33]

Importantly, electric conductivity determines the strength and penetration of dc electric fields inside a given layer under an applied external voltage. In metals, the electric field is screened at the surface of the material (within the outermost 0.5 nm or so)[34] and is zero in its interior. In insulators, the electric field is homogeneous throughout the layer, but its strength is inversely proportional to the layer thickness in a capacitor geometry, while in semiconductors the electric field penetrates several nm from the surface towards the interior, progressively decreasing within the so-called Debye length, which is proportional to the dielectric constant and inversely proportional to the carrier density[35–37] (i.e., $\lambda_D =$

$(\varepsilon k_B T/nq^2)^{1/2}$, where ε, n, q, k_B, and T denote dielectric constant, charge carrier concentration, electron charge, Boltzmann's constant, and absolute temperature[38]). Thus, the magnitude and distribution of electric field inside de voltage-actuated layers, which depends on the electric resistivity or the target material, is likely to determine the strength of the resulting magneto-ionic effects. Remarkably, and in spite of the expected influence of electric resistivity on magneto-ionics, this correlation has been generally overlooked, both in single-layer and in FM/ion-buffer magneto-ionic systems.

In this work, a series of cobalt-nitride films with similar composition (close to equiatomic Co-N, i.e., CoN) but with variable electrical transport properties, are examined. Based on previous reports,[39] the Co-N films were grown at relatively high nitrogen partial pressures to ensure a non-magnetic behavior in the as-prepared state (targeting at either face-centered cubic (FCC) equiatomic CoN or N-rich Co_3N_{1+x} phases).[40,41] Interestingly, previous studies also showed that the crystallite size of FCC CoN can be significantly decreased with the nitrogen partial pressure.[39] Hence, due to enhanced electron scattering at grain boundaries,[42] an increase of electric resistivity with increasing nitrogen partial pressure is expected. The following presents the dramatic effect of the conductivity of the cobalt nitride films on their magneto-ionic behavior, and underscores the important and unexplored role that electrical resistivity plays in magneto-ionics and ionic motion in solids in general.[43,44]

2. Results and Discussion

To investigate the role of electrical transport properties on the magneto-ionic performance, near-stoichiometric cobalt-nitride (CoN) films (85 nm thick) were grown atop Cu (60 nm)/Ti(20 nm)/[1 0 0] oriented Si substrates, using a range of nitrogen partial pressures (0 - 100%). This variation in partial pressure leads to differing degrees of nanocrystallinity, resulting in a range of semiconducting behavior. Samples are denoted as

CoN-VL (very low resistivity), CoN-L (low resistivity), CoN-M (medium resistivity), and CoN-H (high resistivity), in order of increasing resistivity (**Table 1**).

Table 1. Cobalt-nitride samples, nitrogen partial pressure during sputtering, nitrogen concentration, relative lattice expansion, crystalline size, resistivity at room temperature, and relative electric behavior. Lattice parameters and crystallize sizes obtained from Rietveld refinement of the X-ray diffraction patterns[45]. Theoretical lattice parameter of $Fm\bar{3}m$ phase CoN is taken to be a_0 = 4.28 Å (PDF 00-016-0116). Resistivity of as-prepared, pure cobalt is measured to be 11 μΩ • cm at room temperature.

Co-N [units]	P_{N2} [%]	N Concentration [%]	$\Delta a_0/a$ [%]	$\langle D \rangle$ [nm]	ρ [μΩ•cm]	Electric behavior ($d\rho/dT$) [N/A]
CoN-VL	25	35	N/A	<10	156	Metallic
CoN-L	50	50	+3.50	13	411	Metallic/Semiconducting
CoN-M	75	48	+3.06	8	1104	Semiconducting
CoN-H	100	47	+3.02	6	1126	Semiconducting/Insulating

Structural characterization of the samples was carried out using $\theta/2\theta$ X-ray diffraction (XRD). XRD patterns of the as-prepared cobalt-nitride films are shown in **Figure 1**a - **Figure 1**c. Besides the (1 1 1) Cu peak arising from the buffer layer, the CoN-L, CoN-M, and CoN-H films all exhibit a single broad, low intensity peak which is consistent with the (1 1 1) diffraction peak of an expanded $Fm\bar{3}m$ cubic CoN phase (PDF 00-016-0116), evidencing a polycrystalline structure with strong texture (**Figure 1**b). CoN-VL does not present a cubic CoN peak, but rather a broad peak close to the (1 0 1) diffraction peak of Co_3N, suggesting formation of a highly nanocrystalline, nitrogen-rich Co_3N_{1+x} paramagnetic phase (**Figure 1**c).[39,40] The XRD pattern of a metallic Co sample is also shown for comparison. **Table 1** lists the nitrogen content by at. % for each sample, estimated by energy-dispersive X-ray analysis, and the lattice cell parameters and crystallite or grain sizes, determined by Rietveld refinement of the XRD patterns, of all films. The near-stoichiometric CoN films exhibit expanded lattice parameter of ≈ 3% and crystallite sizes ranging from 6 – 13 nm.

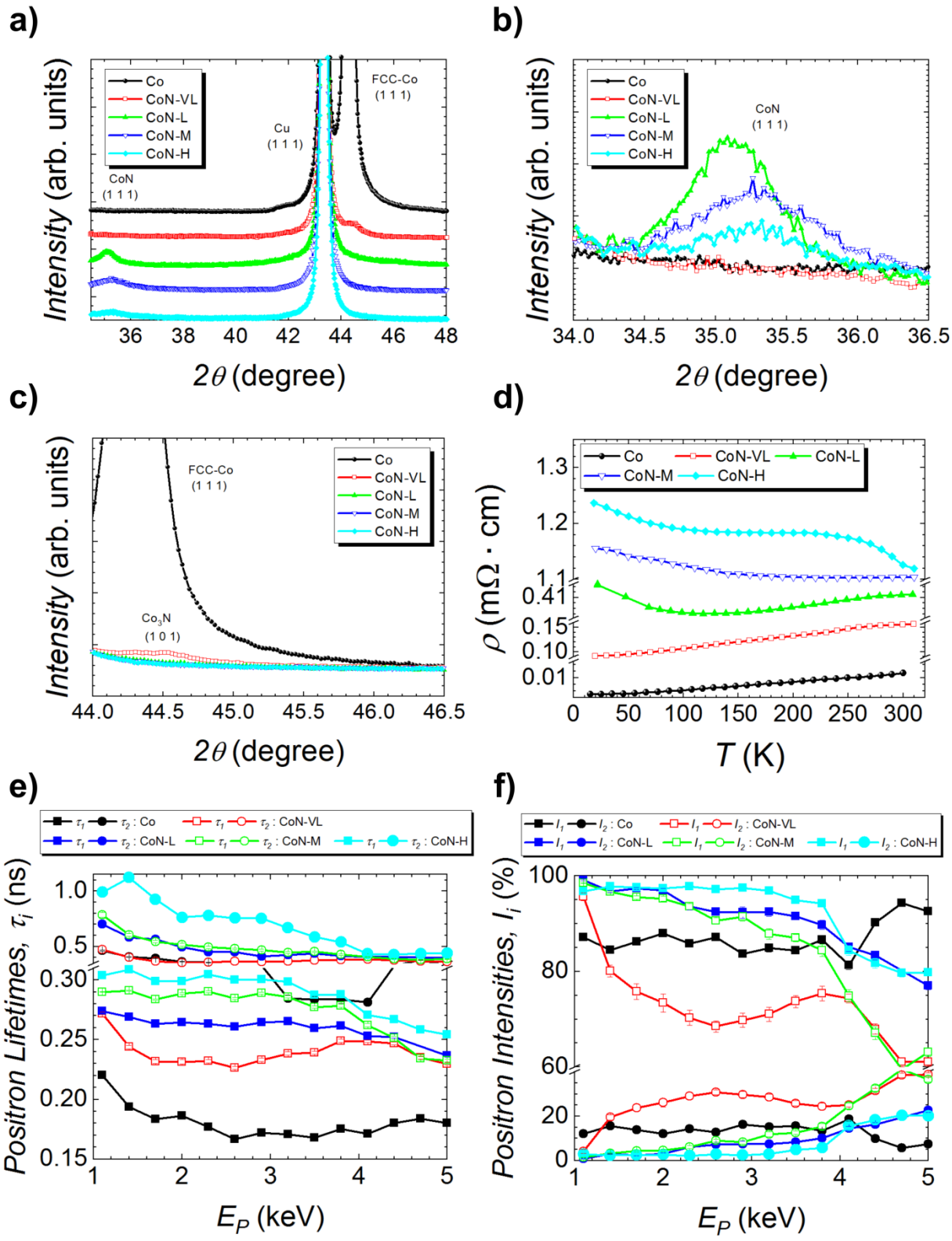

Figure 1. a) $\theta/2\theta$ XRD diffraction patterns of the as-prepared cobalt-nitride films. b-c) Enlarged $\theta/2\theta$ XRD diffraction patterns of near-stoichiometric CoN films (Card number PDF 00-016-0116) and Co_3N[40], respectively. d) Resistivity ρ measured as a function of temperature from 20 K to 300 K, for all cobalt-nitride as-prepared samples. e) Positron lifetime components $\tau_{i=1-2}$. f) Relative intensities $I_{i=1-2}$ as a function of positron implantation energy E_P for all as-prepared cobalt-nitride samples.

Since the ability to hold an electric field and the electric field's strength are crucial components in enabling magneto-ionics, a thorough electric transport characterization was carried out. Resistivity measurements using the van der Pauw configuration were performed as a function of temperature, from 20 to 300 K, for all films (**Figure 1**d). Measurements were also conducted on a purely metallic cobalt film as reference. All measurements were performed on films grown directly on a SiO_2/Si substrate. Decreasing the crystallite size $\langle D \rangle$ clearly increases the resistivity, from ≈ 156 μΩ · cm in CoN-VL to ≈ 1200 μΩ · cm in CoN-H, at room temperature (**Table 1**). The pure cobalt sample shows a monotonic increase of resistivity throughout the temperature range ($d\rho/dT > 0$, where ρ and T are resistivity and temperature, respectively), consistent with metallic behavior (see Supporting Information for plots of individual curves). In CoN-VL, the resistivity is also observed to monotonically increase as well, albeit with a higher overall resistivity than pure cobalt throughout the temperature range due to the presence of nitrogen.[46,47] In CoN-L, a parabolic shape is observed with semiconducting behavior ($d\rho/dT < 0$) appearing below 100 K, and metallic transport ($d\rho/dT > 0$) above 100 K. CoN-M shows an overall semiconducting behavior, while CoN-H behaves similarly, but exhibiting a larger resistivity. Thus, the nitrided samples can be considered to lie on a metallic/semiconducting spectrum, with CoN-VL the most conductive and CoN-H the most resistive (**Table 1**). This suggests that the interplay between nitrogen concentration and microstructure plays an important role in the dielectric.

To further understand the microstructure of each sample, variable energy positron annihilation lifetime spectroscopy (VEPALS) experiments were conducted.[20,48–53] VEPALS data for each as-prepared cobalt-nitride film is presented. Only contributions from τ_1, corresponding to localized vacancies and vacancy clusters, and τ_2, corresponding to a mixture of signals from surface states and grain boundaries are observed (**Figure 1**e and **Figure 1**f).[10] It should be noted that, in the cases of smaller grain sizes (as seen in films sputtered with high nitrogen partial pressure), τ_1 could also represent grain boundaries, as the positrons annihilate

in the largest open volumes, corresponding here to grain boundaries. For E_P > 3.5 keV a change is observed for all parameters of the cobalt-nitride films in **Figure 1**e and **Figure 1**f. This feature is likely a fingerprint of a different defect microstructure (fewer vacancies) appearing deeper in the film, closer to the film/buffer (Cu/Ti) interface. As E_P increases, the signal from the substrate emerges, and each line asymptotically approaches a plateau. In general, positron lifetimes τ_1 and τ_2 are observed to increase with resistivity, indicating a substantial rise of the defect size (see Supporting Information for details). The intensity of τ_1, I_1, is lowest for CoN-VL, then increases for CoN-L and CoN-M, reaching a maximum for CoN-H, with I_2 contributing only residual amounts at high nitrogen concentration and indicating an overall increase in effective defect size (see average positron lifetime in Supporting Information). Thus, as expected, structural defects have a detrimental effect in electric conductivity, in agreement with other systems, such as metals, in which an increase in the number of vacancies leads to larger electronic scattering and so is correlated with larger resistivities.[54]

Figure 2a shows the capacitor (condenser-like) structure used to generate the electric field in all reported measurements. Propylene carbonate (with dissolved Na^+) is used as an anhydrous, polar electrolyte which allows for the application of a uniform voltage by creating an electric double layer (EDL) at the film surface.[10] Voltage is applied while in-plane hysteresis loops are recorded by vibrating sample magnetometry.[18,55–59] In this configuration, a Cu/Ti buffer layer acts as a working electrode and a Pt wire acts a counter electrode, so an out-of-plane electric field is initially generated.[8,59] As-prepared CoN-VL, CoN-L, CoN-M, and CoN-H samples show residual ferromagnetic signals between 1 and 8 emu cm^{-3} (see Supporting Information), with a small initial magnetization present in some samples possibly due to residual off-stoichiometric regions in the film, ferromagnetic impurities in the substrate, or CoN reduction at the CoN/Cu interface. The off-stoichiometry may extend across the film, consistent with the difference in defect structure between the top and bottom of the as-

prepared films observed in the PALS data (**Figure 1**e). In any case, the measured M_S is very low and it corresponds to approximately 0.56% of metallic Co by volume.

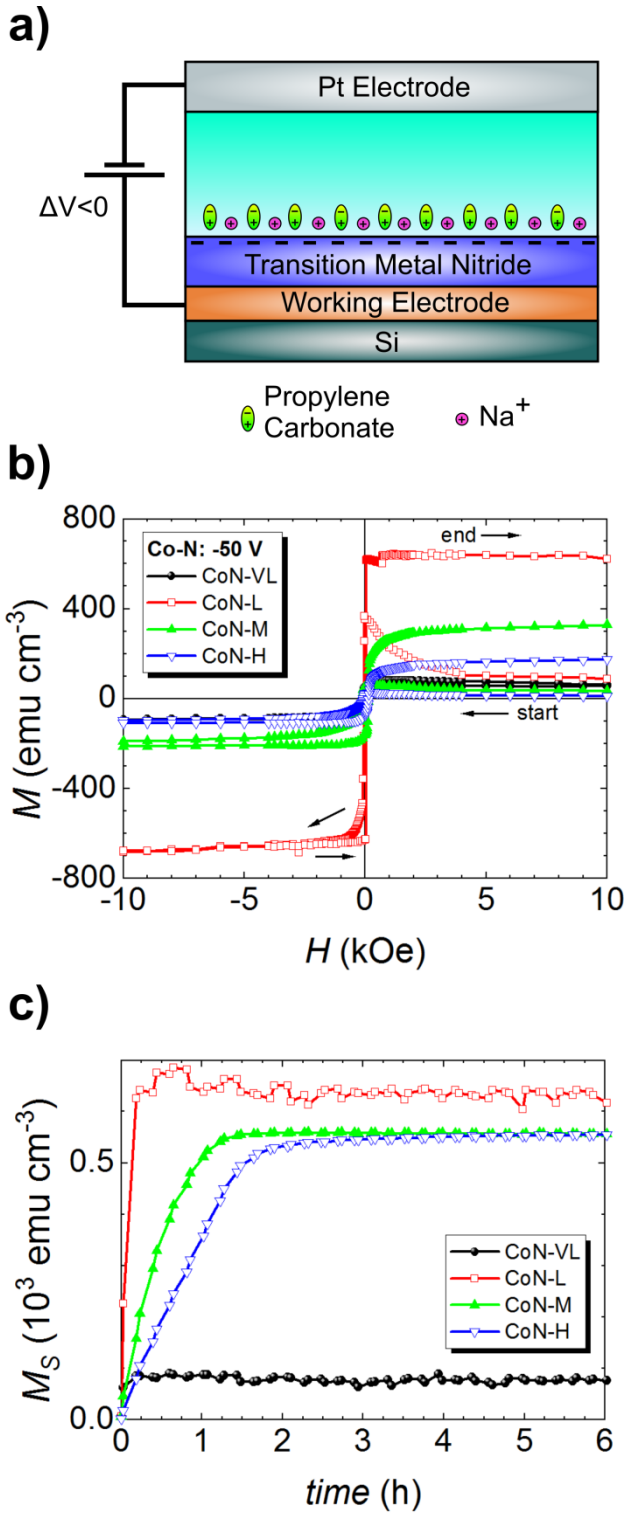

Figure 2. a) Schematic of the condenser-like structure used in each film (electrochemical capacitor configuration). b) First hysteresis loops under -50 V bias for cobalt-nitride films. c) Saturation magnetization (M_S) measured as a function of time for cobalt-nitride films.

To study the magneto-ionic behavior, samples were biased under -50 V during a sequence of 15 magnetic hysteresis loops, lasting 25 min each, and recorded consecutively for the duration of the gating process. During the first loop, the samples show hysteric behavior and a clear increase in magnetization (M_S) as time evolves, indicating clear emergence of a ferromagnetic phase. The first loop measured during each biasing protocol is shown for each film in **Figure 2**b. The magnetization of CoN-VL increases under bias, quickly reaching maximal magnetization (90 emu cm^{-3}) under -50 V gating after one loop (25 min). As reported earlier,[24] CoN-L (denoted in the cited work as 'CoN') shows a tremendous increase in magnetic signal while sweeping through the first quadrant (≈ 6 min) of the hysteresis loop under bias (red loops), and then nearly doubling this value by the end of the first hysteresis loop, to 630 emu cm^{-3}, a factor of nearly 7 when compared to CoN-VL during the same time frame (25 min). CoN-M and CoN-H samples reach values nearly one-half and one-third as large as CoN-L, albeit with a lower rate of increase, as clearly expected from the much milder increase in M as H is swept through the first quadrant (see Supporting Information for several loops plotted in sequence).

To evaluate the rate of increase of the magnetic signal, the saturation magnetization, M_S, is plotted as a function of time for all films (**Figure 2**c); see previous works for further details on quantification[8,24]). Both CoN-VL and CoN-L show a rapid increase (CoN-L especially) and reach magnetic saturation during the first loop, although all samples show clear increases in M_S with time. CoN-VL reaches a maximal value of M_S near 90 emu cm^{-3}, while all other samples reach a maximal M_S greater than 550 emu cm^{-3} (**Table 2**). Both CoN-M and CoN-H reach much higher M_S values than CoN-VL, although less than CoN-L. To elucidate the time scales of increasing ferromagnetism from the as-prepared state, the slope of the magnetization increase during the first 12 min is fitted using a linear regression. The rates obtained during this period were 1012 emu $cm^{-3}\,h^{-1}$ for CoN-VL, 2602 emu $cm^{-3}\,h^{-1}$ for CoN-L, 723 emu $cm^{-3}\,h^{-1}$ for CoN-M, and 427 emu $cm^{-3}\,h^{-1}$ for CoN-H, showing that, under

equivalent voltage, CoN-L generates a ferromagnetic state at a significantly higher rate. Further examination of the evolution of the magnetic and structural properties of the samples under biasing similar to those done in previous works[8,24] (coercivity, squareness, slope of the hysteresis loops, XRD) can be found in Supporting Information.

Table 2. Magneto-ionic rates under -50 V bias during the first 12 min, saturation magnetization, loop squareness, normalized slope at the coercive field, and coercive field after 6 hours. All values above measured under -50 V bias.

Co-N [units]	dM_S/dt [emu cm^{-3} h^{-1}]	M_S [emu cm^{-3}]	M_R/M_S [%]	$M_S^{-1}\, dM/dH \,@\, H_C$ [kOe^{-1}]	H_C [Oe]
CoN-VL	1012	90	84	21	65
CoN-L	2602	637	96	97	17
CoN-M	723	558	83	18	153
CoN-H	427	556	80	16	167

Remarkably, the film with the highest magneto-ionic rate (CoN-L) does not possess either the largest resistivity or the largest number of defects. Here, contrary to what has been reported in previous works, the amount of grain boundaries and the nanocrystallinity of the CoN-M and CoN-H samples, on their own, do not correlate with the magneto-ionic effects.[10] In fact, the higher resistivity in CoN-M and CoN-H causes a decrease in magneto-ionic response. This suggests that there are important trade-offs to consider in N-based target materials between microstructure, nitrogen concentration, bonding, and the electric field distribution inside the films to achieve maximized magneto-ionic rates. As expected, field penetration depends heavily on the semiconductor charge density.[60] To estimate the field profile inside the film, COMSOL simulations were performed for an 85 nm semiconductor film with a range of charge carrier densities (n = 10^{15} - 10^{21}) at the moment (t = 0) a bias -50 V is applied via an electric double layer, before ion motion begins (**Figure 3**). The Debye length is examined for a relative permittivity value of ε_r = 10, representing a typical value for transition metal nitrides.[60,61] The calculated electric fields are normalized to the field of a

highly resistive film ($n = 10^5$ carriers) taken to be insulating. The carrier density is found to modify the penetration depth of the field, ranging from < 1 nm up to > 10 nm. In metallic-like CoN-VL film (with a larger number of charge carriers), the electric field is very high at the interface with the propylene carbonate, but goes to zero very rapidly within the first 1-2 nm of the surface. In this case, the applied voltage is able to induce N ion motion only at the interface with the electrolyte, which leaves most of the CoN layer unaffected, thus rendering very little magneto-ionic effects beyond a quickly achieved maximum (in agreement with the results shown in **Figure 2**b). Conversely, in the most insulating film CoN-H (the lowest charge carrier density), the applied voltage produces a field which extends deep into the film, but with relatively low strength. In the intermediate case (semiconducting CoN layers with intermediate resistivity values), a substantially larger electric field is obtained near the interface, propagating >10 nm inwards, affecting a larger volume of the magneto-ionic layer than CoN-VL. This gradient in the electric field may contribute to the observed planar migration front in CoN-L.[24] Also, the defect gradient along depth, as observed by PALS, together with the smaller, isotropic grains (as compared with columnar grains in Co_3O_4 [8,10]), may promote the planar ionic front seen in CoN.[24] It should be noted that the physical picture presented in **Figure 3** shows the penetrating field *E* after the charge carriers have redistributed along the surface under an applied voltage, which alone does not capture all the observed behavior.

Beyond the initial steady state electric field depth, the dynamics of ionic motion (how N ions are transported, and charge carriers in the denitrided area redistributed) must play a key role in magneto-ionic performance. For intermediate resistivity values, electric field is strong enough to eventually produce nitrogen ionization and ion migration to the electrolyte, thereby leaving positively-charged nitrogen vacancies behind. As ionization proceeds nitrogen vacancies flow inwards towards the negatively charged electrode surface and an equivalent opposite nitrogen ionic current occurs towards the EDL. Nitrogen ions are driven

outside the material layer-by-layer (onion-like) via plane wave-like migration, leaving behind an electrochemical gradient that may vary at grains and grain boundaries, impacting the penetrating field distribution and local ion redistribution. Note that as ion migration proceeds, the CoN films resistive profile will change, similar to other systems undergoing resistive changes under ionic movement.[60] During ion migration, semiconducting CoN becomes more electrically conductive due to the formation of metallic Co clusters and, as the carrier density increases, the Debye length decreases. This process progresses until the nitrogen is exhausted or the induced metallic cobalt manages to screen the applied electric field. This is a dynamic and coupled effect which depends on electric resistivity and the screening length. Indeed, as ionic flow progresses and the penetration depth of the electric field progressively decreases, the field reaches less of the layer interior, leading to a decrease in magneto-ionic effects, eventually reaching an equilibrium in the generated magnetization, as observed as a saturation after several hours of biasing.[24] Note that the attained value of M_S is close to 700 emu/cm^3 (**Figure 2**d), which roughly corresponds to half of the 1422 emu cm^{-3} M_S of pure Co,[62] suggesting that the layer becomes highly nanoporous since,[24] given the absence of N (as assessed by EELS), no contribution from Co_4N or Co_3N_{1+x} phases is expected in the magnetic properties.

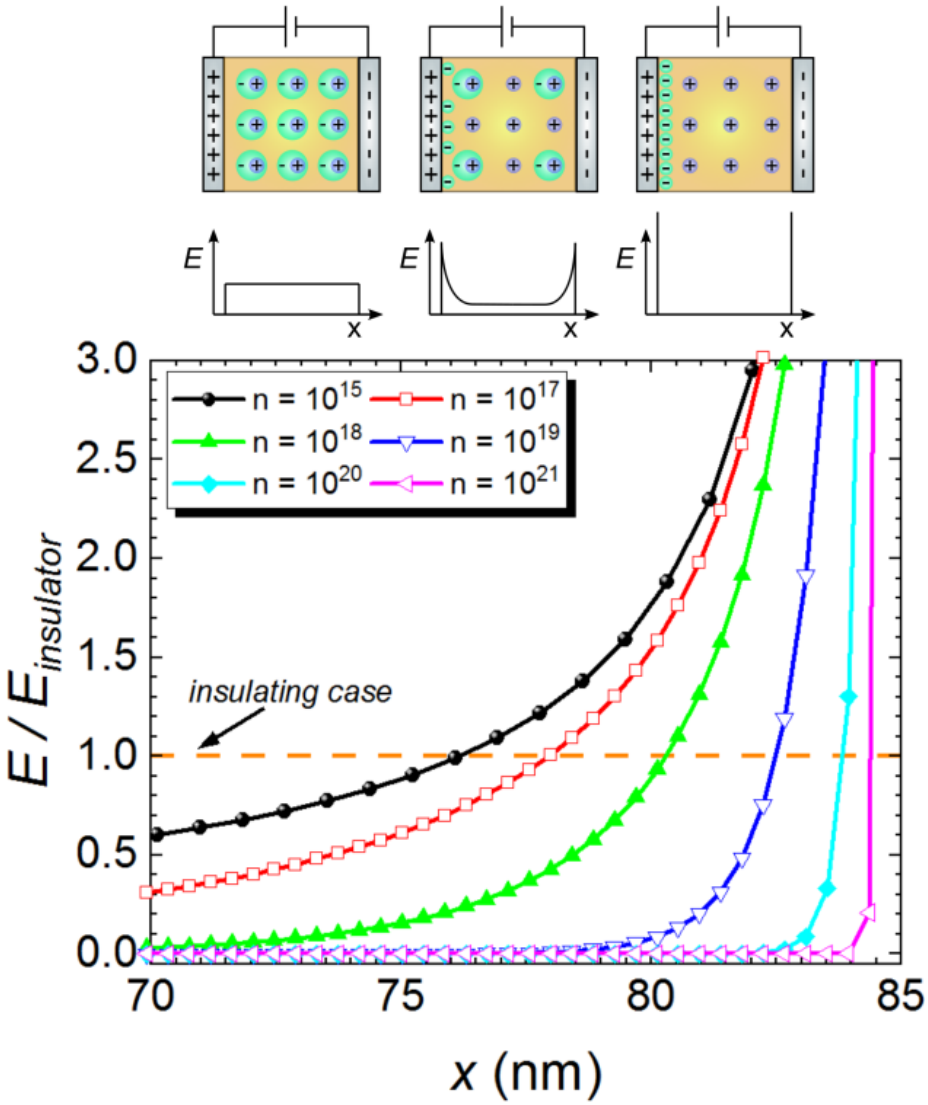

Figure 3. Debye screening lengths calculated for charge carrier densities ranging from n = 10^{15} - 10^{21} (least to most insulating cases), calculated for a typical relative permittivity for transition metal nitrides of ε_r = 10 and normalized to the resistive case. Simple schematics above show representative expected field extensions in the ideal insulating (left), semiconducting (center), and metallic cases (right).

The general role of resistivity in the generated electric field must be refined, also taking into account also the strength of the CoN atomic bonding[63], to better understand the dissociation of the CoN molecules at the proximity of the electrolyte. The bonding increases in strength in the more resistive bonds, such as CoN-H. More conductive bonds, such as those in CoN-VL, are typically associated with weaker atom-atom bonds, which can facilitate ionic motion. In particular, CoN-VL shows mild increase in M_S before quickly flattening, while the

more resistive CoN-L shows a large increase in magnetization, much greater than CoN-VL. However, even more resistive CoN-M and CoN-H both show milder increases in M_S than the relatively conducting CoN-L. This suggests a balance must be reached between the extension of the applied field into the film and the bond strength holding ions in place, which can be tuned via defects and crystallinity, with electrical transport serving as an indicator of performance. The influence of the detailed grain structure on the field and ion movement profiles, presumably with grains with more coordinated structures and larger resistivity and grain boundaries less coordinated and more conductive, is an interesting point that deserves further future investigation.

3. Conclusion

Electrical resistivity is a key parameter controlling magneto-ionic motion, which can be used as an indicator of attainable magneto-ionic effects because it crucially merges the interplay between transition metal-nitrogen bonding, microstructure, size and type of defects, and the strength of the electric field and its corresponding penetration depth into the target material. The more conductive CoN films are found to exhibit very limited magneto-ionic response due to electric-field screening, while the most insulating CoN films show sub-optimal ionic motion. The best balance is achieved in Co-N films with intermediate resistivity values. This work has implications not only in nitrides, but also applies more generally to other single-layer semiconductors, and perhaps also provides a powerful parameter of control in bilayered systems (such as Co/GdO_x or Co/HfO_x) that can be used to optimize magneto-ionic effects via electrical transport tuning.

4. Experimental Section/Methods

Sample Preparation: 85 nm thick CoN films were grown by reactive sputtering on boron-doped, highly conducting [100], 500 μm thick silicon wafers, previously coated with 20 nm of titanium and 60 nm of copper. The copper was masked during deposition to serve as a working electrode. The expanded CoN films were grown in a home-made triode sputtering system with a base pressure in the range of 10^{-8} Torr. Ultra-high vacuum was ensured to minimize oxygen contamination. The target to substrate distances were around 10 cm and the sputtering rate around 1 Å/s. CoN films were grown in a range of nitrogen partial pressure (100% Ar / 0% N_2, 75% Ar / 25% N_2, 50% Ar / 50% N_2, 25% Ar / 75% N_2, 0% Ar / 100% N_2) environments, at a total pressure of 8×10^{-3} Torr.

Magnetic Characterization: Magneto-electric measurements were performed by vibrating sample magnetometry while electrolyte-gating the film in a capacitor configuration at room temperature. The samples are mounted in a homemade electrolytic cell containing anhydrous propylene carbonate with sodium cation solvated species (5 – 25 ppm). The Na^+ solvated species in the electrolyte are present to react with any trace amounts of water in the propylene carbonate[64]. The magnetic properties of the samples were measured in-plane while applying different voltages. This was done using a Micro Sense (LOT – Quantum Design) magnetometer, with maximum field of 2 T. Voltages were applied using an Agilent B2902A power supply, between the sample working electrode and the counter electrode, as demonstrated in previous works[10,59,64]. The magnetic signal was normalized to the volume sample exposed to the electrolyte during the gating process. All measured hysteresis loops were background-corrected, carried out at high fields (always above the saturation field), to eliminate linear contributions (paramagnetic or diamagnetic signals).

Structural and Compositional Measurements: $\theta/2\theta$ X-ray diffraction patterns were recorded on a Materials Research Diffractometer (MRD) from the Malvern PANalytical company, equipped with a PIXcel^{1D} detector, using Cu K_α radiation. XRD patterns were

analyzed using Rietveld refinement to obtain lattice cell parameters and crystallize size (average size of coherently diffracting sample domains)[45].

High resolution transmission electron microscopy (HRTEM), high-angle annular dark-field scanning transmission electron microscopy (HDAAF-STEM) and electron energy loss spectroscopy (EELS) were performed on a TECNAI F20 HRTEM/STEM microscope operated at 200 kV. Cross-sectional lamellae were prepared by focused ion beam and placed onto a Cu transmission electron microscopy grid.

Transport Measurements: Both cobalt-nitride and iron-nitride films were deposited onto high resistivity Si substrates. Resistivity values were acquired from 30 to 300 K, all using the van der Pauw configuration.

Variable Energy Positron Annihilation Lifetime Spectroscopy: Variable energy positron annihilation lifetime spectroscopy (VEPALS) measurements were conducted at the mono-energetic positron source (MePS), an end station of the radiation source ELBE (Electron Linac for beams with high Brilliance and low Emittance) at Helmholtz-Zentrum Dresden-Rossendorf (Germany)[48] using a $CeBr_3$ detector coupled to a digital lifetime spectrometer with a homemade software employing a SPDevices ADQ14DC-2X with 14 bit vertical resolution and 2GS s^{-1} (GigaSamples per second) horizontal resolution and with a time resolution function down to about 0.205 ns. The resolution function required for spectrum analysis uses two Gaussian functions with distinct intensities depending on the positron implantation energy, E_p, and appropriate energy shifts. All spectra measured contain at least 10^7 counts.

Simulations of Electric Field Distribution: The distribution of electric field inside the actuated CoN layers was simulated as a function of electric resistivity using the COMSOL software. Note that the electric double layer was modelled as an ultra-thin (0.5 nm) insulating film[65] with relative dielectric constant $\varepsilon_r = 1$. This value is much smaller than the permittivity of propylene carbonate in absence of electric field and it is in line with the

expected ε_r values under the action of the strong electric fields generated in the EDL[66,67], which could easily exceed 50 V nm^{-1}. The dielectric constant of CoN was chosen to be around $\varepsilon/\varepsilon_r = 10$, in line with reports on the literature for several transition metal nitrides[60,61].

Supporting Information
Supporting Information is available from the Wiley Online Library or from the author.

Acknowledgements
Financial support by the European Research Council (SPIN-PORICS 2014-Consolidator Grant, Agreement Nº 648454, and the MAGIC-SWITCH 2019-Proof of Concept Grant, Agreement Nº 875018), the Spanish Government (MAT2017-86357-C3-1-R), the Generalitat de Catalunya (2017-SGR-292 and 2018-LLAV-00032) and the European Regional Development Fund (MAT2017-86357-C3-1-R and 2018-LLAV-00032) is acknowledged. This work was partially supported by the Impulse-und Net-working fund of the Helmholtz Association (FKZ VH-VI-442 Memriox), and the Helmholtz Energy Materials Characterization Platform (03ET7015). The PALS measurements were carried out at ELBE at the Helmholtz-Zentrum Dresden-Rossendorf e. V., a member of the Helmholtz Association. Ll. Abad thanks MINECO for a Ramón y Cajal Contract (RYC-2013-12640). J. Sort thanks the Spanish Fábrica Nacional de Moneda y Timbre (FNMT) for fruitful discussions.

Received: ((will be filled in by the editorial staff))
Revised: ((will be filled in by the editorial staff))
Published online: ((will be filled in by the editorial staff))

References

[1] C. Song, B. Cui, F. Li, X. Zhou, F. Pan, *Prog. Mater. Sci.* **2017**, *87*, 33.

[2] J. M. Hu, C. W. Nan, *APL Mater.* **2019**, *7*, 80905.

[3] S. Vasala, A. Jakob, K. Wissel, A. I. Waidha, L. Alff, O. Clemens, *Adv. Electron. Mater.* **2020**, *6*, 1900974.

[4] A. J. Tan, M. Huang, S. Sheffels, F. Büttner, S. Kim, A. H. Hunt, I. Waluyo, H. L. Tuller, G. S. D. Beach, *Phys. Rev. Mater.* **2019**, *3*, 064408.

[5] S. Dasgupta, B. Das, M. Knapp, R. A. Brand, H. Ehrenberg, R. Kruk, H. Hahn, *Adv. Mater.* **2014**, *26*, 4639.

[6] U. Bauer, L. Yao, A. J. Tan, P. Agrawal, S. Emori, H. L. Tuller, S. Van Dijken, G. S. D. Beach, *Nat. Mater.* **2015**, *14*, 174.

[7] L. Baldrati, A. J. Tan, M. Mann, R. Bertacco, G. S. D. Beach, *Appl. Phys. Lett.* **2017**, *110*, 012404.

[8] J. de Rojas, A. Quintana, A. Lopeandía, J. Salguero, J. L. Costa-Krämer, L. Abad, M. O. Liedke, M. Butterling, A. Wagner, L. Henderick, J. Dendooven, C. Detavernier, J. Sort, E. Menéndez, *Adv. Funct. Mater.* **2020**, *30*, 2003704.

[9] A. J. Tan, M. Huang, C. O. Avci, F. Büttner, M. Mann, W. Hu, C. Mazzoli, S. Wilkins, H. L. Tuller, G. S. D. Beach, *Nat. Mater.* **2019**, *18*, 35.

[10] A. Quintana, E. Menéndez, M. O. Liedke, M. Butterling, A. Wagner, V. Sireus, P. Torruella, S. Estradé, F. Peiró, J. Dendooven, C. Detavernier, P. D. Murray, D. A. Gilbert, K. Liu, E. Pellicer, J. Nogues, J. Sort, *ACS Nano* **2018**, *12*, 10291.

[11] A. Molinari, H. Hahn, R. Kruk, *Adv. Mater.* **2019**, *31*, 1806662.

[12] M. Gößler, M. Albu, G. Klinser, E. M. Steyskal, H. Krenn, R. Würschum, *Small* **2019**, *15*, 1904523.

[13] D. A. Gilbert, J. Olamit, R. K. Dumas, B. J. Kirby, A. J. Grutter, B. B. Maranville, E. Arenholz, J. A. Borchers, K. Liu, *Nat. Commun.* **2016**, *7*, 11050.

[14] D. A. Gilbert, A. J. Grutter, E. Arenholz, K. Liu, B. J. Kirby, J. A. Borchers, B. B. Maranville, *Nat. Commun.* **2016**, *7*, 12264.

[15] K. Duschek, M. Uhlemann, H. Schlörb, K. Nielsch, K. Leistner, *Electrochem. commun.* **2016**, *72*, 153.

[16] S. Dasgupta, B. Das, Q. Li, D. Wang, T. T. Baby, S. Indris, M. Knapp, H. Ehrenberg, K. Fink, R. Kruk, H. Hahn, *Adv. Funct. Mater.* **2016**, *26*, 7507.

[17] F. Ibrahim, A. Hallal, B. Dieny, M. Chshiev, *Phys. Rev. B* **2018**, *98*, 214441.

[18] C. Navarro-Senent, J. Fornell, E. Isarain-Chávez, A. Quintana, E. Menéndez, M. Foerster, L. Aballe, E. Weschke, J. Nogués, E. Pellicer, J. Sort, *ACS Appl. Mater. Interfaces* **2018**, *10*, 44897.

[19] C. Li, G. D. Love, T. W. Lyons, D. A. Fike, A. L. Sessions, C. Li, G. D. Love, T. W.

Lyons, D. A. Fike, A. L. Sessions, X. Chu, *Science (80-.).* **2016**, *328*, 80.

[20] E. H. Khan, M. H. Weber, M. D. McCluskey, *Phys. Rev. Lett.* **2013**, *111*, 017401.

[21] W. Eerenstein, N. D. Mathur, J. F. Scott, *Nature* **2006**, *442*, 759.

[22] K. Duschek, A. Petr, J. Zehner, K. Nielsch, K. Leistner, *J. Mater. Chem. C* **2018**, *6*, 8411.

[23] C. Bi, Y. Liu, T. Newhouse-Illige, M. Xu, M. Rosales, J. W. Freeland, O. Mryasov, S. Zhang, S. G. E. Te Velthuis, W. G. Wang, *Phys. Rev. Lett.* **2014**, *113*, 267202.

[24] J. de Rojas, A. Quintana, A. Lopeandía, J. Salguero, B. Muñiz, F. Ibrahim, M. Chshiev, A. Nicolenco, M. O. Liedke, M. Butterling, A. Wagner, V. Sireus, L. Abad, C. J. Jensen, K. Liu, J. Nogués, J. L. Costa-Krämer, E. Menéndez, J. Sort, *Nat. Commun.* **2020**, *11*, 5871.

[25] M. Kimura, S. Inoue, T. Shimoda, T. Sameshima, *Japanese J. Appl. Physics, Part 1 Regul. Pap. Short Notes Rev. Pap.* **2001**, *40*, 49.

[26] R. Landauer, in *AIP Conf. Proc.*, AIP Publishing, **2008**, pp. 2–45.

[27] C. Durkan, M. Welland, *Phys. Rev. B - Condens. Matter Mater. Phys.* **2000**, *61*, 14215.

[28] R. Resta, S. Sorella, *Phys. Rev. Lett.* **1999**, *82*, 370.

[29] W. Kohn, *Phys. Rev.* **1964**, *133*, A171.

[30] Á. M. Pendás, J. M. Guevara-Vela, D. M. Crespo, A. Costales, E. Francisco, *Phys. Chem. Chem. Phys.* **2017**, *19*, 1790.

[31] J. Szczyrbowski, K. Schmalzbauer, *J. Phys. F Met. Phys.* **1986**, *16*, 2079.

[32] A. F. Mayadas, M. Shatzkes, *Phys. Rev. B* **1970**, *1*, 1382.

[33] L. Moraga, C. Arenas, R. Henriquez, S. Bravo, B. Solis, *Phys. B Condens. Matter* **2016**, *499*, 17.

[34] N. D. Ashcroft, N. W.; Mermin, *Solid State Physics*, New York : Holt, Rinehart And Winston, **1976**.

[35] T. T. Tsong, *Surf. Sci.* **1979**, *81*, 28.

[36] E. Stern, R. Wagner, F. J. Sigworth, R. Breaker, T. M. Fahmy, M. A. Reed, *Nano Lett.* **2007**, *7*, 3405.

[37] P. Debye, E. Hückel, *Phys. Zeitschrift* **1923**, *24*, 185.

[38] J. Mizsei, *Sensors Actuators B. Chem.* **1995**, *23*, 173.

[39] R. Gupta, N. Pandey, A. Tayal, M. Gupta, *AIP Adv.* **2015**, *5*, 097131.

[40] K.-H. Mader, F. Thieme, A. Knappwost, *Zeitschrift für Anorg. und Allg. Chemie* **1969**, *366*, 274.

[41] K. Suzuki, T. Kaneko, H. Yoshida, H. Morita, H. Fujimori, *J. Alloys Compd.* **1995**, *224*, 232.

[42] I. Krylov, E. Zoubenko, K. Weinfeld, Y. Kauffmann, X. Xu, D. Ritter, M. Eizenberg, *J. Vac. Sci. Technol. A* **2018**, *36*, 051505.

[43] D. S. Jeong, H. Schroeder, R. Waser, *Phys. Rev. B* **2009**, *79*, 195317.

[44] R. Waser, R. Dittmann, G. Staikov, K. Szot, *Adv. Mater.* **2009**, *21*, 2632.

[45] L. Lutterotti, P. Scardi, *J. Appl. Crystallogr.* **1990**, *23*, 246.

[46] S. H. Cho, K. R. Yoon, K. Shin, J. W. Jung, C. Kim, J. Y. Cheong, D. Y. Youn, S. W. Song, G. Henkelman, I. D. Kim, *Chem. Mater.* **2018**, *30*, 5941.

[47] P. Chen, K. Xu, Y. Tong, X. Li, S. Tao, Z. Fang, W. Chu, X. Wu, C. Wu, *Inorg. Chem. Front.* **2016**, *3*, 236.

[48] A. Wagner, M. Butterling, M. O. Liedke, K. Potzger, R. Krause-Rehberg, *AIP Conf. Proc.* **2018**, *1970*, 040003.

[49] J. V. Olsen, P. Kirkegaard, N. J. Pedersen, M. Eldrup, *Phys. Status Solidi Curr. Top. Solid State Phys.* **2007**, *4*, 4004.

[50] R. Krause-Rehberg, H. S. Leipner, **1999**, XV.

[51] F. Tuomisto, I. Makkonen, *Rev. Mod. Phys.* **2013**, *85*, 1583.

[52] K. Wada, T. Hyodo, *J. Phys. Conf. Ser.* **2013**, *443*, 012003.

[53] M. O. Liedke, W. Anwand, R. Bali, S. Cornelius, M. Butterling, T. T. Trinh, A.

Wagner, S. Salamon, D. Walecki, A. Smekhova, H. Wende, K. Potzger, *J. Appl. Phys.* **2015**, *117*, 163908.

[54] T. Broom, *Nature* **1953**, *171*, 1104.

[55] M. Weisheit, S. Fähler, A. Marty, Y. Souche, C. Poinsignon, D. Givord, *Science (80-.).* **2007**, *315*, 349.

[56] S. Robbennolt, E. Menéndez, A. Quintana, A. Gómez, S. Auffret, V. Baltz, E. Pellicer, J. Sort, *Sci. Rep.* **2019**, *9*, 10804.

[57] S. Robbennolt, A. Nicolenco, P. Mercier Fernandez, S. Auffret, V. Baltz, E. Pellicer, E. Menéndez, J. Sort, *ACS Appl. Mater. Interfaces* **2019**, *11*, 37338.

[58] C. Leighton, *Nat. Mater.* **2019**, *18*, 13.

[59] C. Navarro-Senent, A. Quintana, E. Menéndez, E. Pellicer, J. Sort, *APL Mater.* **2019**, *7*, 030701.

[60] M. Gong, J. Gao, D. Shen, P. Li, W. Tong, C. Liu, *J. Magn. Magn. Mater.* **2020**, *514*, 167246.

[61] M. González, A. Ibarra, *Diam. Relat. Mater.* **2000**, *9*, 467.

[62] B. D. Cullity, C. D. Graham, in *Introd. to Magn. Mater.*, **2009**.

[63] J. Häglund, A. Fernndez Guillermet, G. Grimvall, M. Körling, *Phys. Rev. B* **1993**, *48*, 11685.

[64] A. Quintana, J. Zhang, E. Isarain-Chávez, E. Menéndez, R. Cuadrado, R. Robles, M. D. Baró, M. Guerrero, S. Pané, B. J. Nelson, C. M. Müller, P. Ordejón, J. Nogués, E. Pellicer, J. Sort, *Adv. Funct. Mater.* **2017**, *27*, 1.

[65] K. K. Mahanta, G. C. Mishra, M. L. Kansal, *Appl. Clay Sci.* **2012**, *59–60*, 1.

[66] L. Yang, B. H. Fishbine, A. Migliori, L. R. Pratt, *J. Chem. Phys.* **2010**, *132*, 044701.

[67] H. Wang, L. Pilon, *J. Phys. Chem. C* **2011**, *115*, 16711.

[68] D. L. Leslie-Pelecky, R. D. Rieke, *Chem. Mater.* **1996**, *8*, 1770.

[69] W. Anwand, G. Brauer, M. Butterling, H. R. Kissener, A. Wagner, *Defect Diffus.*

Forum **2012**, *331*, 25.

[70] M. J. Puska, R. M. Nieminen, *J. Phys. F Met. Phys.* **1983**, *13*, 333.

[71] A. P. Seitsonen, M. J. Puska, R. M. Nieminen, *Phys. Rev. B* **1995**, *51*, 14057.

Voltage control of ionic motion (magneto-ionics) can potentially serve as the basis for future magnetic devices and technologies. By examining the magneto-ionic effects in a series of CoN films with varying electronic transport properties, resistivity is shown to be critical to performance and serves as a powerful, tunable parameter which can be used to optimize magneto-ionic effects.

Julius de Rojas, Joaquín Salguero, Alberto Quintana, Aitor Lopeandia, Maciej O. Liedke, Maik Butterling, Ahmed G. Attallah, Eric Hirschman, Andreas Wagner, Llibertat Abad, José L. Costa-Krämer*, Jordi Sort* and Enric Menéndez*

The critical role of electrical resistivity in magneto-ionics